

## DUST AND THE INFRARED KINEMATIC PROPERTIES OF EARLY-TYPE GALAXIES

JULIA D. SILGE AND KARL GEBHARDT

Astronomy Department, University of Texas at Austin, 1 University Station C1400, Austin, TX 78712  
dorothea@astro.as.utexas.edu, gebhardt@astro.as.utexas.edu

*Draft version November 1, 2018*

### ABSTRACT

We have obtained spectra and measured the stellar kinematics in a sample of 25 nearby early-type galaxies (with velocity dispersions from less than 100 km s<sup>-1</sup> to over 300 km s<sup>-1</sup>) using the near-infrared CO absorption bandhead at 2.29 μm. Our median uncertainty for the dispersions is ~10%. We examine the effects of dust on existing optical kinematic measurements. We find that the near-infrared velocity dispersions are in general smaller than optical velocity dispersions, with differences as large as 30%. The median difference is 11% smaller, and the effect is of greater magnitude for higher dispersion galaxies. The lenticular galaxies (18 out of 25) appear to be causing the shift to lower dispersions while the classical ellipticals (7 out of 25) are consistent between the two wavelength regimes. If uniformly distributed dust causes these differences, we would expect to find a correlation between the relative amount of dust in a galaxy and the fractional change in dispersion, but we do not find such a correlation. We do see correlations both between velocity dispersion and CO bandhead equivalent width, and velocity dispersion and Mg<sub>2</sub> index. The differences in dispersion are not well explained by current models of dust absorption. The lack of correlation between the relative amount of dust and shift in dispersion possibly suggests that dust does not have a similar distribution from galaxy to galaxy. The CO equivalent widths of these galaxies are quite high ( $\gtrsim 10 \text{ \AA}$  for almost all), requiring the light at these wavelengths to be dominated by very cool stars.

*Subject headings:* galaxies: elliptical and lenticular, cD — galaxies: kinematics and dynamics

### 1. INTRODUCTION

Before infrared detectors became available, the amount of dust in a galaxy was estimated from patchy, optically visible obscuration. However, since dust emits in the far infrared, observing in that part of the spectrum gives a better measure of the total amount of dust. Recent far-infrared observations have shown that galaxies, even ellipticals and bulges of galaxies, contain an unexpectedly large amount of dust (Goudfrooij & de Jong 1995). This dust may bias the optical region by skewing photometric and/or kinematic data through absorption and scattering. Observing in the near infrared allows us to minimize these problems. Many groups have studied the photometric bias introduced by dust, and here we study its kinematic effect. Previous attempts at studying kinematic dust effects were limited to those galaxies with obvious concerns. There has been no systematic investigation based on a general galaxy population. Our goal here is to quantify these effects by studying a subset of galaxies that are thought to have minimal dust problems: early-type galaxies. Also, observing at these longer wavelengths traces the older, redder stellar population and minimizes effects due to recent star formation. Thus, kinematics in this spectral regime should produce the best measure of the underlying stellar potential of the galaxy. As infrared instrumentation and telescopes become more efficient, this region is quickly becoming very important. As a first step, we must characterize the IR features for kinematic analysis. Furthermore, analysis of these possible biases and problems is important to accurately interpret the data we will soon have from very large optical samples.

Observations using the Infrared Astronomical Satellite (IRAS) have shown that galaxies, even those previously thought to be practically dust-free such as ellipticals and bulges of galaxies, can contain a large amount of dust. Dust masses determined from far infrared IRAS flux densities are about a factor

of 10 higher than those estimated from optically visible patches and lanes (Goudfrooij & de Jong 1995). More sophisticated estimates of the dust mass using submillimeter data give values even higher (Kwan & Xie 1992; Wiklind & Henkel 1995). There is much more dust out there than is apparent when observing in the visible. Goudfrooij & de Jong (1995) explain this by suggesting that most of this dust exists as a diffusely distributed component, which would be undetectable in the optical regime.

How does dust affect our measurements of galaxies? Models of elliptical galaxies considering only dust absorption show effects on both the photometric and kinematic data. The photometric effects include a global attenuation, strong extinction in the central regions, and an increasing apparent core radius (Baes & Dejonghe 2000). The core radius is one of the primary parameters used to study galaxy correlation functions and according to these models appears larger than its true value because the luminosity profile is flattened towards the center by the dust. The core radius can increase by over 25% for an optical depth  $\tau \approx 2$  (a moderate amount of dust), an important effect considering the small amount of scatter in the galaxy correlation functions. The effects of absorption on kinematic properties (Baes et al. 2000), calculated by building semi-analytic dusty galaxy models and then modeling the synthetic data assuming no dust, depend on the shape of the velocity dispersion tensor of the input model. For radial and isotropic orbital structures, the inferred dynamical mass is significantly underestimated while the inferred orbital structure is mostly unaffected. For an optical depth  $\tau \approx 2$ , the dynamical mass appears 20% smaller. For galaxies with tangential orbital structures, the dynamical mass is not affected much but the inferred orbital structure appears more radial, even for small amounts of dust. Both these effects are due to dust preferentially obscuring light from high-velocity regions of the galaxies. Baes et al. (2000) find that dust absorption does not significantly af-

fect the velocity dispersion but that the dynamical structure is not correctly recovered. Baes & Dejonghe (2001, 2002) construct models with both dust absorption and dust scattering (using Monte Carlo methods), and find different effects on the observed kinematics which still depend on the orbital structure of the input galaxy. At small radii, dust causes the central dispersion to appear smaller for radial and isotropic galaxies and to appear larger for tangential galaxies. This effect is small; an optical depth  $\tau \approx 2$  causes a change of a few percent. There are dramatic changes at large radii, however. The attenuation by dust, mostly the scattering, results in high-velocity wings in the line-of-sight velocity distribution (LOSVD) in the outer parts of the galaxy. For  $\tau \approx 1$ , the projected dispersion at large radii can increase by over 40%. Both these effects (at small and large radii) are caused by the scattering of light from high-velocity stars into lines of sight at which such stars do not exist.

Galaxies which are visibly dusty pose a less subtle problem. Although they, too, may have a diffusely distributed gas component, the high level of obscuration of visible light from patches and lanes hinders optical spectroscopy of the galaxies. There are a significant number of galaxies out there for which the existing kinematic data are suspect and untrustworthy because of visible dust. Dust lanes are already seen in about half of all ellipticals (Kormendy & Djorgovski 1989; Lauer et al. 1995; van Dokkum & Franx 1995; Rest et al. 2001; Tran et al. 2001), with higher detection rates as search techniques (especially spatial resolution) improve. These galaxies are often not included in kinematic studies because data for them are unreliable, introducing potential bias into current kinematic samples. It is important to observationally constrain how observed galaxy kinematics are being affected or biased by interstellar dust.

Galaxy kinematics are measured in the optical using several different spectral features. The most common include the H and K lines (Ca II) near 4000 Å, the Mg *b* lines near 5175 Å, and the Ca II triplet near 8500 Å. Studies comparing kinematic measurements made using different features, such as Nelson & Whittle (1995), do not find significant differences between them, although Barth, Ho, & Sargent (2002) find the Mg *b* lines are sensitive to template mismatch and the details of the fitting procedure while the Ca II triplet is much more robust. All these spectral features may be affected by dust to some extent. Dust is very opaque in the *B* band where the H and K lines are located and absorbs less efficiently at longer wavelengths. At 5000 Å, dust absorption is 75% of that in *B* and decreases to 40% in *I* where the Ca II triplet is located. Moving to a feature like the Ca II triplet certainly reduces problems associated with extinction, but effects from dust can be further minimized by moving to longer wavelengths. The extinction in the *K* band is only 7% of that at *B* (Gaffney et al. 1995; Baes & Dejonghe 2002).

In this project, we measure the stellar kinematics in a sample of 25 nearby early-type galaxies using the *K*-band CO absorption bandhead. Using wavelengths this long will allow us to avoid dust absorption and gain a more accurate understanding of the kinematics of these galaxies. This sample will provide a check of possible kinematic biases using optical light. Calibrating the CO bandhead for galaxy kinematic measurements is an important goal of this study. Working in the near infrared holds great promise for both scientific motivations and future instrumentation. Specifically, adaptive optics, in which the optical system is continually adjusted to compensate for the effects of seeing, work best in the near infrared. The longer wavelengths in this part of the spectrum allow less stringent requirements

on optics adjustment. Using the CO bandhead will optimize kinematic analysis for adaptive optics.

This technique can also be extended to other scientific questions. Our current understanding of the kinematics of galaxies has led to the study of relations between different characteristics of galaxies in  $\kappa$ -space (i.e. Fundamental Plane, Faber-Jackson relation, Tully-Fisher relation; e.g. Burstein et al. 1997). These relations have been derived using data from optical stellar emission lines, so dusty, complicated, messy galaxies are not included in the analyses. The galaxy sample itself may be biased because of the exclusion of these galaxies. Also, if bulges and elliptical galaxies have a diffusely distributed dust component, these analyses may suffer from important problems due to internal absorption and extinction. Observing in the *K* band would avoid these problems.

This paper is organized as follows: Section 2 presents the data, Section 3 discusses our analysis techniques, Section 4 presents our results for the infrared kinematic measurements and how these results compare to other data for these galaxies, and Section 5 summarizes.

## 2. DATA

### 2.1. The Sample

Table 1 shows the 25 galaxies in this project. The sample contains ellipticals and lenticulars, and has redshifts less than 5000 km s<sup>-1</sup>. Our sample is made largely of galaxies from Tonry et al. (2001). Tonry et al. (2001) present distance moduli for 300 nearby galaxies from surface brightness fluctuations. This presents an ideal sample to draw from for this study; these galaxies are systems with bulges (mostly E and S0, with some S), are essentially complete to a redshift of 1000 km s<sup>-1</sup>, and have well-determined distances (which are necessary to calculate the dust mass and other physical properties). The galaxy type and heliocentric velocity (from NED), distance modulus (from Tonry et al. 2001), and the calculated distance are listed in Table 1. The sample contains about twice as many S0 galaxies as classical ellipticals, which is reflective of the galaxies in the SBF sample at these redshifts. For the few galaxies in this sample that are not in Tonry et al. (2001), the distance is calculated from the recessional velocity using  $H_0 = 70$  km s<sup>-1</sup> Mpc<sup>-1</sup>. This is relatively accurate because the few galaxies without distance moduli have redshifts  $> 2000$  km s<sup>-1</sup>. These galaxies have a range of IRAS dust characteristics, from no detectable dust to several million solar masses of dust (see Section 3.3). All galaxies have associated IRAS fluxes from Knapp et al. (1989) and the 1994 correction to those data (available at <http://cdsweb.u-strasbg.fr/CDS.html>).

### 2.2. The CO Bandhead

The 2.29  $\mu\text{m}$  (2-0) <sup>12</sup>CO absorption bandhead from evolved red stars is the strongest absorption feature in galactic spectra in the 1–3  $\mu\text{m}$  range. This is the optimal range for studying stellar kinematics because it is long enough to minimize extinction from dust but short enough to avoid dilution of the stellar continuum by hot dust (Gaffney et al. 1995). The feature is in a dark part of the infrared sky spectrum and is intrinsically sharp and deep, making it very sensitive to stellar motions (Lester & Gaffney 1994).

The CO bandhead is present in late-type stars, increasing in strength with decreasing effective temperature or increasing radius. The CO bandhead has been used to measure the stellar kinematics of galaxies in recent years, but only in galaxies

such as starbursts and mergers where optical kinematic measurements are seriously hindered (Tamura et al. 1991; Gaffney et al. 1993; Doyon et al. 1994; Lester & Gaffney 1994; Shier et al. 1994, 1996; Puxley et al. 1997). There are no velocity dispersion measurements from the CO bandhead for galaxies which are well-studied in the optical, and thus there is no information on possible differences between optical and infrared kinematics.

### 2.3. Observations and Data Reduction

Observations were taken during 27 nights in six observing runs between December 2000 and January 2002. We use CoolSpec (Lester et al. 2000), a near-infrared grating spectrometer, on the 2.7-m telescope at McDonald Observatory to measure the stellar kinematics in our sample. CoolSpec has a  $256 \times 256$  HgCdTe NICMOS III detector array. Using a 240 l/mm grating and  $1.8'' \times 90''$  slit, our spectral resolution is 2300, measured from calibration lamp lines. This gives a full width half maximum (FWHM) resolution of approximately  $130 \text{ km s}^{-1}$ , which allows us to study galaxies with velocity dispersions down to approximately  $50 \text{ km s}^{-1}$ . Resolving the dispersions of early-type galaxies is easily within reach of this observational set-up. We have obtained spectra for about 40 galaxies, 27 of which are early-type. We have successfully extracted the line-of-sight velocity distribution for 25 of these galaxies, which make up the sample for this project. The other two galaxies were too large on the chip to allow for good sky subtraction.

The spatial and spectral scale are  $0''.35 \text{ pixel}^{-1}$  and  $24.6 \text{ km s}^{-1} \text{ pixel}^{-1}$ , respectively. The latter gives a spectral range of just under  $0.05 \mu\text{m}$ , which is large enough to provide good coverage of the CO bandhead and continuum on both sides. Technically, the true continuum is not seen redward of  $2.29 \mu\text{m}$  because of the long wing of CO absorption that makes the bandhead, but this is not important for our fitting technique.

We observed multiple types of stars along with the galaxies; G and K giants were observed as examples of templates for the velocity fitting and A dwarfs were observed to obtain the shape of a “flat” spectrum. These dwarf stars have nearly featureless spectra in this region (Wallace & Hinkle 1997) and are extremely important to the data reduction. The imager in CoolSpec is cooled separately from the dispersive optics, requiring the use of a filter just in front of the detector to reduce the thermal background incident on the array. This filter shape must be removed during data reduction. Also, the atmospheric absorption at McDonald Observatory appears to vary on a timescale inconvenient for these observations. Atmospheric transmission calculations (Gaffney et al. 1995) indicate that telluric absorption is dominated by  $\text{CH}_4$ , not  $\text{H}_2\text{O}$ , blueward of  $2.34 \mu\text{m}$ , implying that atmospheric absorption should not vary much with time. This is not consistent with our experience at McDonald Observatory, however; the shape of a single A star spectrum can change significantly during a night. For both of these reasons, it is very important to take a careful (and frequent) measure of the detailed spectral shape of the filter/sky to be able to remove this shape from the observed spectra. We choose A dwarfs spatially near each galaxy and observe one before and after each galaxy/template observation. We also observe an A dwarf sometime in the middle of long galaxy observations.

The observations are made by dithering the telescope  $30''$  across the slit to measure the sky at the same slit position in alternating exposures. Individual exposures are 120 seconds for the galaxies and ten seconds for the stars. Total integra-

tion times for the galaxies vary from about one hour to almost five hours. Galaxies that require very long integration times or that are at low declinations are observed during several nights to maintain reasonable airmasses. The slit is rotated to the position angle of the galaxy major axis as quoted in the RC3. Ar and Ne (or Xe for some runs) emission lamps calibrate the wavelengths of the exposures. Calibration exposures are taken every 24 minutes; the wavelength solution drifts significantly with time. The telescope guides on either the galaxy itself or a nearby star (if available) using the optical dichroic mirror autoguider. No attempt is made to flux calibrate the spectra since we are mainly concerned with the kinematic analysis.

Data reduction proceeds in several steps. First, the images are rectified spectrally using the arc lamp emission lines. We find that there is an additive constant across the entire chip which varies from exposure to exposure, so this dark current is measured for each exposure and then subtracted out. We measure this in the same location for each exposure, in pixels without signal from either slit position. We make a master background image for each galaxy by masking out the object spectrum in each individual exposure—half of which have the object at one position on the slit, and half of which have it at another position—calculating the biweight, a robust estimator of the mean (Beers et al. 1990), of all the exposures. Galaxies observed on different nights, for long periods of time, or during particularly humid nights required the construction of several different background images to get good subtraction. We find that we must choose carefully how much exposure time to average together: long enough to make a smooth, robust background image but short enough to allow for changes in the sky. This background image is then subtracted from each individual exposure. The images are next shifted to the same wavelength solution; we interpolate between the two closest calibrations to find a good estimate of the wavelength solution and then shift all the images from one observing run to the same solution. This step must be done after the background subtraction or the image of the seams between the detector’s four quadrants does not subtract out well. All the images are then shifted so that the center of the galaxy in each image is aligned; we calculate the biweight of all the processed images to make one image for the galaxy. The one-dimensional spectra are extracted from the two-dimensional images for basically the entire galaxy; we choose the number of columns to extract to maximize signal-to-noise. For the sample, this varies between  $4''$  and  $20''$ . For some high S/N galaxies, we are also able to extract spatially resolved spectra. The stellar spectra are reduced in a similar manner.

To remove telluric absorption and the filter shape, the galaxy and template stellar spectra must be divided by a “flat” spectrum. After trying several approaches, we obtained the best results by using the following procedure. First, all the A dwarfs from a run are averaged together to make a smooth, high S/N sky spectrum. Figure 1 shows such an average spectrum for the December 2001 run. The galaxy, template, and individual “flat” spectra are divided by this smooth spectrum. For some galaxies and template stars, this provides good flattening. For the rest, the spectrum is divided by a version of the A dwarf nearest in time to that observation, smoothed by the resolution element to reduce noise. Dividing by only an individual A star does not give results as good as the smooth sky spectrum made from many A stars because of the fluctuations in the individual spectra. These individual stars change because of fluctuations

in the sky, not because of problems with S/N.

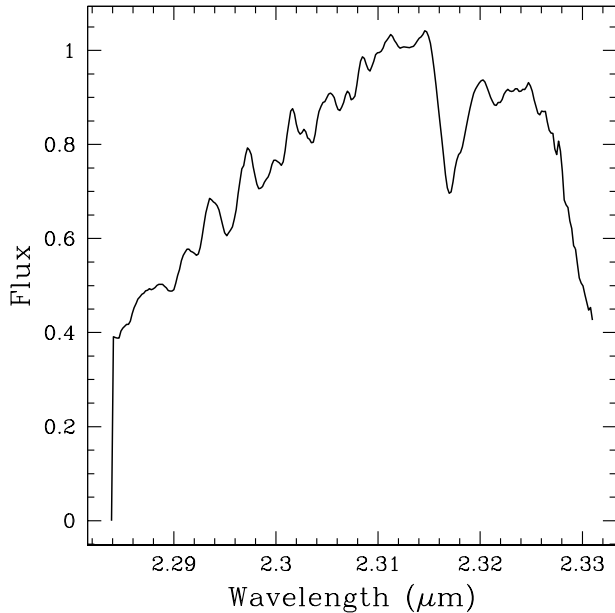


FIG. 1.— Average “flat” spectrum for December 2001 run. This spectrum is constructed from over 60 observations of A stars over the course of the run, as described in the text. The features in this spectrum are real and not due to noise.

### 3. ANALYSIS

#### 3.1. *Extracting the Velocity Distribution*

A galaxy spectrum is the convolution of the line-of-sight velocity distribution (LOSVD) with an average stellar spectrum. Figure 2 shows several examples; the dotted spectrum with many small features is that of a typical K giant while the smooth spectra are the stellar spectrum convolved with three Gaussian LOSVDs (with dispersions of 100, 200, and 300 km s<sup>-1</sup>). This figure shows the smoothing and broadening due to the internal velocities. The bandhead is obviously very broad, but its sharp blue edge allows us to measure accurately the kinematics.

There are several techniques used to obtain the internal kinematic information from a galaxy spectrum. The cross-correlation technique (Tonry & Davis 1979) extracts the velocity dispersion utilizing the cross-correlation function of the galaxy spectrum and template stellar spectrum; the width of the peak of the cross-correlation function provides the dispersion. This technique requires correct subtraction of the continuum and is sensitive to template mismatch. The Fourier quotient technique (Sargent et al. 1977) uses the result of the convolution theorem: the Fourier transform of the LOSVD is the quotient of the Fourier transform of the galaxy spectrum and the Fourier transform of the template spectrum. Both of these techniques fit the kinematics in Fourier space; however, the spectrum can also be fit directly in pixel space, which is the approach taken here.

We use the fitting technique of Gebhardt et al. (2000a), deconvolving the spectrum using a maximum penalized likelihood estimate to obtain a nonparametric LOSVD. An initial velocity profile is chosen and this profile is convolved with a stellar template spectrum. The residuals to the galaxy spectrum are calculated and the velocity profile is changed to minimize the residuals and provide the closest match to the observed galaxy spectrum.

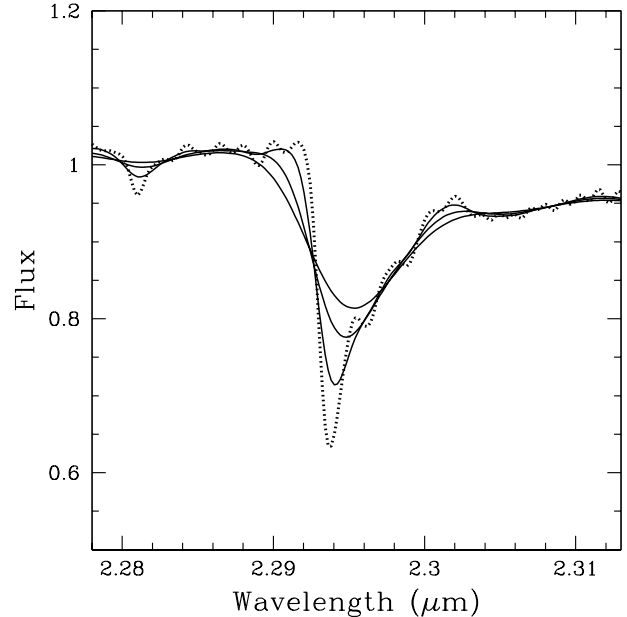


FIG. 2.— CO bandhead in a typical mid-K giant (dotted line with high frequency features) at our resolution and then convolved with Gaussian LOSVDs with dispersions of 100, 200, and 300 km s<sup>-1</sup> (solid spectra). The equivalent width for this star is 13.4 Å.

The choice of template star proves to be important for the fitting results. Previous work in the CO bandhead used mostly K and M giant stars as templates, but it is not clear that this is a correct choice. We use the atlas of Wallace & Hinkle (1997) to test the effect of stellar type on the fitting results. The equivalent width of the CO bandhead is a function of the effective temperature and surface gravity of the star; either increasing the surface gravity or decreasing the temperature increases the equivalent width. Figure 3 shows our calculations of the equivalent widths of most of the stars of Wallace & Hinkle (1997); these trends are evident.

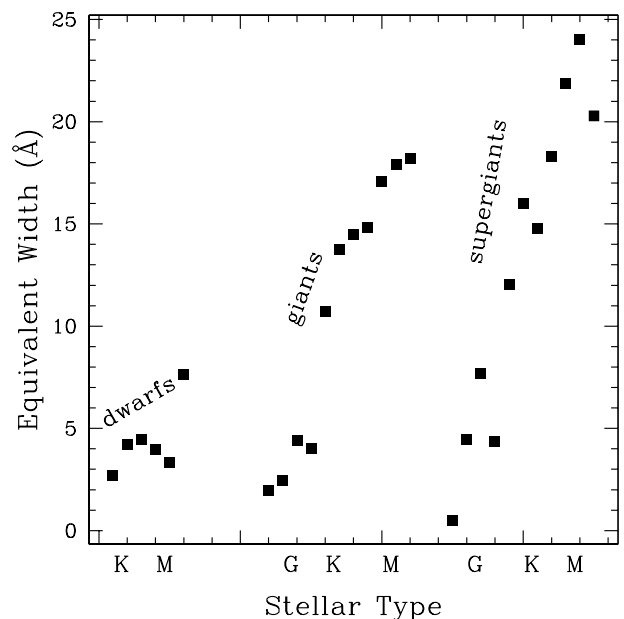


FIG. 3.— Equivalent width of the CO bandhead as a function of spectral type. These are our measurements of equivalent width for the stellar spectra of Wallace & Hinkle (1997).

We have found that the dispersion measured by the fitting program depends on the template spectrum chosen for the fitting. Figure 4 illustrates this point for NGC 1161. The dispersion measured for this galaxy increases as the equivalent width of the template star’s bandhead increases. The  $\chi^2$  for each of these fits is shown as well and is quite high for most, indicating poor fits. One template with an equivalent width near the galaxy’s equivalent width appears to give a significantly better fit. Other galaxies show a similar trend. The shape of the CO bandhead must be a function of equivalent width. To obtain a reliable dispersion measurement, we give the fitting program a variety of template stellar spectra and allow it to vary the weights given to the different stars to obtain the best fit. As a result, along with the LOSVD information, the fitting program also provides stellar population information. We have explored the effect on the fitting of using stars of the same equivalent width but different stellar types; this does not seem to be important. It is the equivalent width of the template that counts, not the details of the spectral type. We choose eight stars from Wallace & Hinkle (1997) to use as our available templates. These stars have a range of equivalent widths, ranging from less than 5 Å to over 20 Å. The best fit almost always gives most of the weight to a few of the template stars. We have also used template stars observed with the same instrumental setup used for the galaxies. We find similar results using these stars but the better S/N and larger equivalent width variation of Wallace & Hinkle (1997) make that dataset more useful. These spectra have a somewhat higher spectral resolution than ours, so before using them as stellar templates we have carefully convolved them to our spectral resolution.

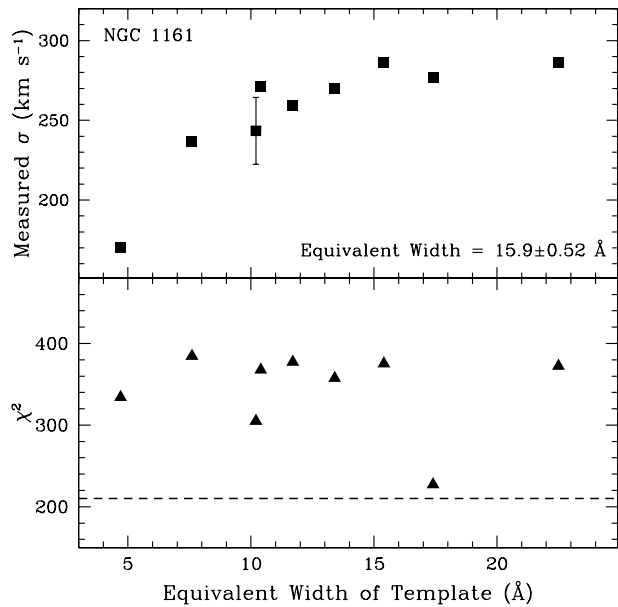


FIG. 4.— Dispersion measured by the fitting program for NGC 1161 as a function of the equivalent width of the input template star and the  $\chi^2$  for each fit. The error bar shown is representative for all these dispersions. For comparison, the dispersion measured for NGC 1161 allowing the program to choose templates is 274 km s<sup>-1</sup> with  $\chi^2 = 211$ , lower than any of the fits using individual stars. The dashed line shows the  $\chi^2$  for an acceptable fit, given the 210 constraints.

Because of this equivalent width effect, the continuum choice may skew the velocity dispersion measurement. If the red continuum chosen is too blue, i.e. encroaching on the bandhead, the measured equivalent width will be too low and the resulting

measured velocity dispersion will be lower than the true dispersion. We have tested the effects of the continuum choice and find that this is not a large source of uncertainty. We convolved a stellar template with Gaussian LOSVDs and made different choices for the red continuum. The effect was as expected but was not large. Only very obviously bad choices for the red continuum cause a 10% decrease in the dispersion; more realistic mistakes in the continuum choice cause decreases of less than 5%, smaller than most of our error bars. We have also examined the effects of changing the continuum definition in the actual galaxy spectra; the changes in the LOSVD fits and velocity dispersions are very small.

This fitting technique obtains a nonparametric LOSVD; no a priori assumptions about the shape of the LOSVD are made (except that it is nonnegative in all bins). To measure a dispersion from this nonparametric LOSVD, we fit a Gauss-Hermite polynomial to it and use the second moment as the dispersion. We can also fit a Gaussian LOSVD directly to the spectrum. Galaxies in the sample with low S/N required the assumption of a Gaussian LOSVD in order to achieve a sensible velocity distribution. The fitting program can get lost in residual space when there are too many free parameters for the level of noise in the spectrum, and this was the case for the lower S/N galaxies in our sample. We compared the derived nonparametric and Gaussian LOSVDs for galaxies with higher S/N and found good agreement between them. Figure 5 shows the results for all 25 sample galaxies and the derived velocity dispersion for each galaxy. The noisy line is the observed spectrum for each galaxy and the smooth line is the template stellar spectrum convolved with the derived LOSVD.

The uncertainties for these galaxies are determined using the Monte Carlo bootstrap approach of Gebhardt et al. (2000a). For each galaxy, a template spectrum is convolved with the derived LOSVD to make an initial galaxy spectrum. We then generate 100 realizations of the galaxy spectrum by randomly drawing the flux values at each wavelength from a Gaussian distribution. The mean of this distribution is the value of the initial template spectrum convolved with the LOSVD (i.e. the smooth line in Fig. 5) and the standard deviation is the root-mean-square of the initial fit. These 100 synthetic galaxy spectra are then deconvolved to determine the LOSVDs. These LOSVDs provide a distribution of values for each velocity bin which allow us to estimate the uncertainty and examine any bias in the dispersion. To generate the 68% confidence bands, we choose the 16% to 84% values from the 100 realizations. The median of the distribution determines any potential bias from the initial fit. Figure 6 shows how the S/N of the observed galaxy spectrum affects the percent accuracy to which we can measure the dispersion. Using this technique and spectral feature, 10% accuracy in the velocity dispersion requires S/N per pixel of about 25 or 30.

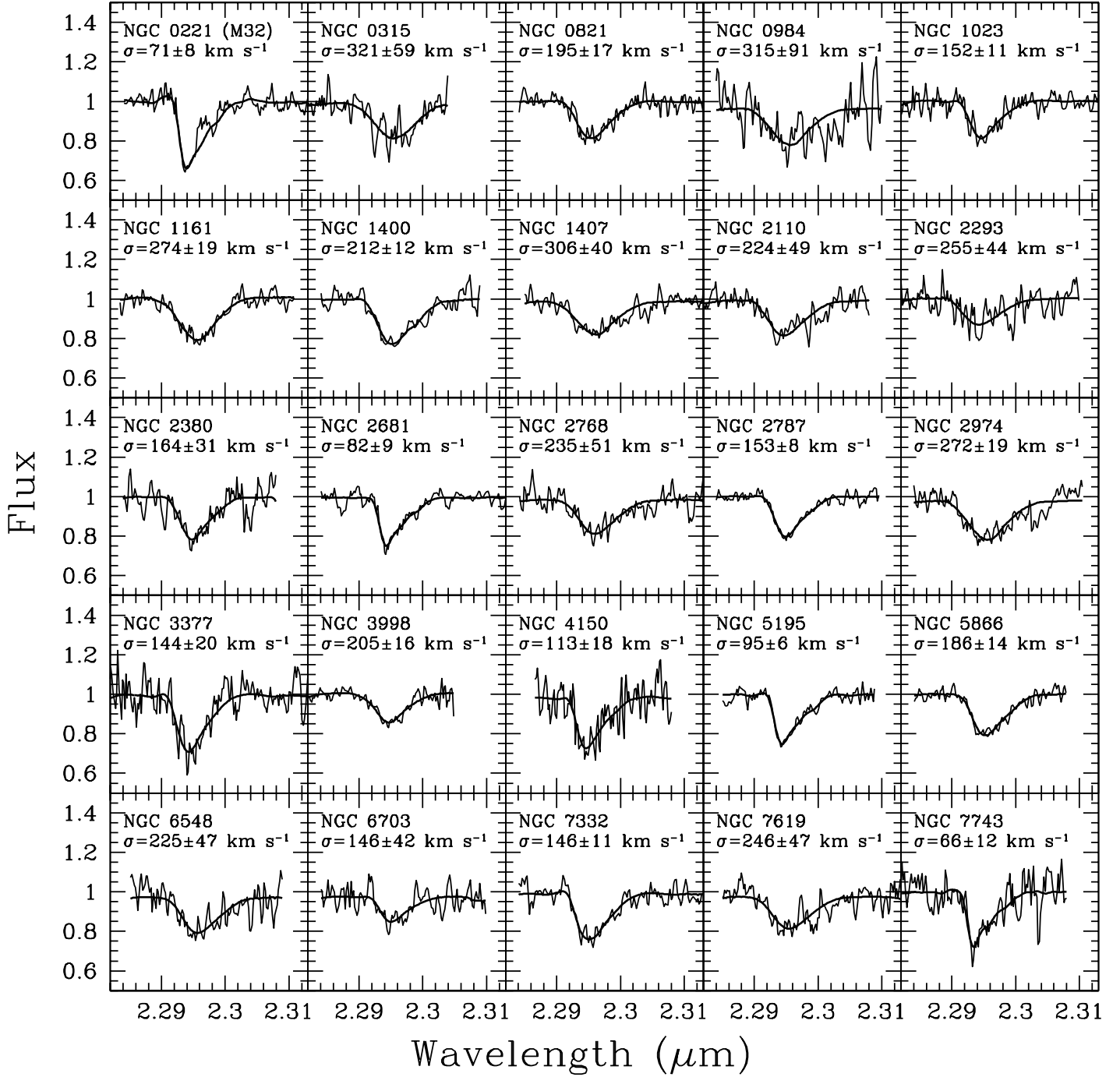


FIG. 5.— Rest-frame spectra for galaxies observed at McDonald Observatory (noisy line) and for the template stellar spectrum convolved with the derived velocity distribution (smooth line). The derived velocity dispersion and its 68% uncertainty are reported for each galaxy.

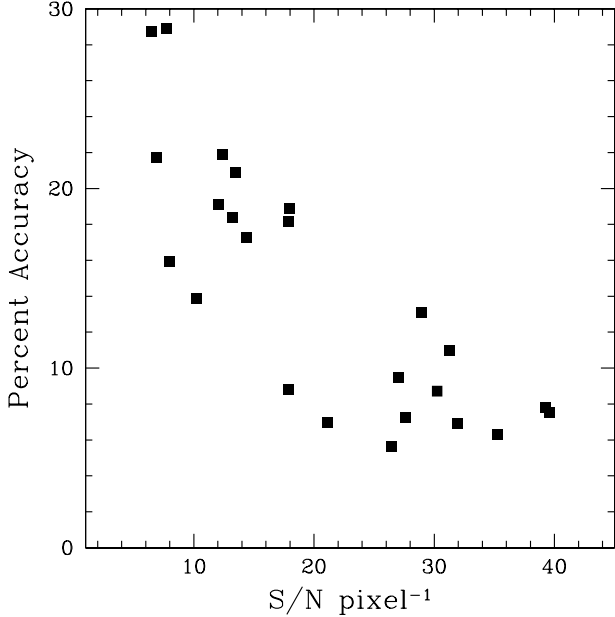


FIG. 6.— Percent accuracy to which we measure the velocity dispersion using the fitting technique described in the text versus measured S/N per pixel of the spectra. Our wavelength scale is  $1.9 \text{ \AA}/\text{pixel}$ .

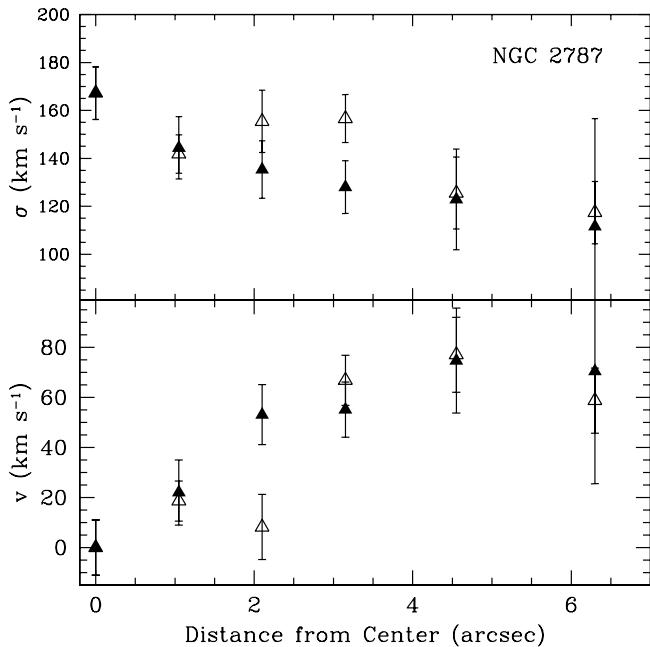


FIG. 7.— Velocity dispersion and velocity curves for NGC 2787. The open and filled triangles are for the opposite sides of the galaxy. The velocity dispersion derived for the entire galaxy as described in the text is  $153 \pm 8 \text{ km s}^{-1}$ .

It is possible to obtain spatially resolved kinematics from these data as well, when the S/N for the galaxy is high enough. Figure 7 shows the variation of velocity and velocity dispersion with distance from the center of the galaxy for NGC 2787. In the center regions, we extract spectra of approximately the width of the seeing disk for that night and in the outer regions, we increase the number of pixels extracted to keep the S/N high enough to derive the LOSVD. The velocity dispersion curve is peaked in the center of the galaxy, and both sides of the galaxy show the same decrease. The velocity dispersion measured for the entire galaxy (extracted to maximize S/N) is  $153 \pm 8 \text{ km}$

$\text{s}^{-1}$ . Figure 7 shows that this is the value achieved by the velocity dispersion curve between 0.5 and 1.5 arcseconds away from the center.

### 3.2. Equivalent Widths

The equivalent width of the  $2.29 \mu\text{m}$  CO feature can be used to quantify stellar population effects in these galaxies. To measure the equivalent width, we define continuum on both sides of the feature and fit a straight line between these two points. In the rest frame of the galaxy, the continuum on the blue is defined to be the median between  $2.287$  and  $2.290 \mu\text{m}$ , and on the red between  $2.304$  and  $2.307 \mu\text{m}$  (about 15 pixels on each side). We use the velocity information from the LOSVD fitting procedure to shift the galaxy spectra to their rest frames. We measure the area between the continuum line and the observed spectrum between  $2.290$  and  $2.304 \mu\text{m}$ , and divide by the continuum to find the equivalent width. Since true continuum is not seen redward of the feature, we choose to define the quasi-continuum where the spectrum again becomes nearly horizontal.

We calculate uncertainties for the equivalent width using the same Monte Carlo method used for the velocity dispersion. We generate 100 realizations of each galaxy spectrum from the fit to the observed spectrum found by the LOSVD fitting procedure, with noise chosen to match the S/N of the observed spectrum. We measure the equivalent width of these 100 synthetic galaxy spectra and use this distribution of equivalent widths to estimate the uncertainty and examine bias. We choose the 16% to 84% values from this distribution for our 68% uncertainty, and use the median to look for bias. We also measure the equivalent width of the (noiseless) fit from the LOSVD extraction, which matches the median from the Monte Carlo simulations well.

There does not appear to be any bias for most of these galaxies, i.e. the equivalent width of the observed spectrum is close to (within the uncertainty of) the median from the Monte Carlo simulations. For three galaxies, this is not the case. Messier 32, NGC 984, and NGC 2974 all have features in their spectra that cause a significant difference between the equivalent widths of the observed spectra and the fits (see Fig. 5 to see these differences). These features are likely due to variability in sky absorption which was not well-removed by our flattening procedure, combined with low S/N for NGC 984 and NGC 2974. (See later section on Messier 32 for more discussion.) For these galaxies, we choose to use the equivalent width of the fit, basically the same as the median from the Monte Carlo simulations, as our value for the equivalent width. We believe these values are more reliable than the values compromised by sky variability and noise issues.

These measurements of the equivalent width must be corrected for the effect of the galaxy dispersion. The velocity broadening throws equivalent width outside of our chosen measuring region, especially on the sharp blue edge. To calculate this correction, we take spectra for several types of stars, with equivalent widths ranging from about  $7 \text{ \AA}$  to almost  $20 \text{ \AA}$ , and convolve them with Gaussian velocity distributions of different dispersions. We then measure the equivalent widths of these convolved spectra in the same way we measure the galactic spectra in order to see how much we should correct our real equivalent width measurements. The dispersion correction for the CO bandhead agrees well between the different stars used, and we find this correction to be rather large, about 20% for  $300 \text{ km s}^{-1}$ . This is typical for some features used in optical regions (Trager et al. 1998). The correction we use, found by fitting a

cubic polynomial to the data from the convolved stellar spectra, is  $\frac{EW_{observed}}{EW_{actual}} = 1 - 1.853 \times 10^{-4} \sigma + 1.287 \times 10^{-6} \sigma^2 - 9.695 \times 10^{-9} \sigma^3$  where  $EW_{observed}/EW_{actual}$  is the ratio of observed and actual equivalent widths and  $\sigma$  is the velocity dispersion measured in  $\text{km s}^{-1}$ . Figure 8 illustrates this dispersion correction. The symbols show the fractional change in equivalent width for each star as a function of velocity dispersion, and the line shows the fit mentioned above used to correct our galaxy equivalent width measurements.

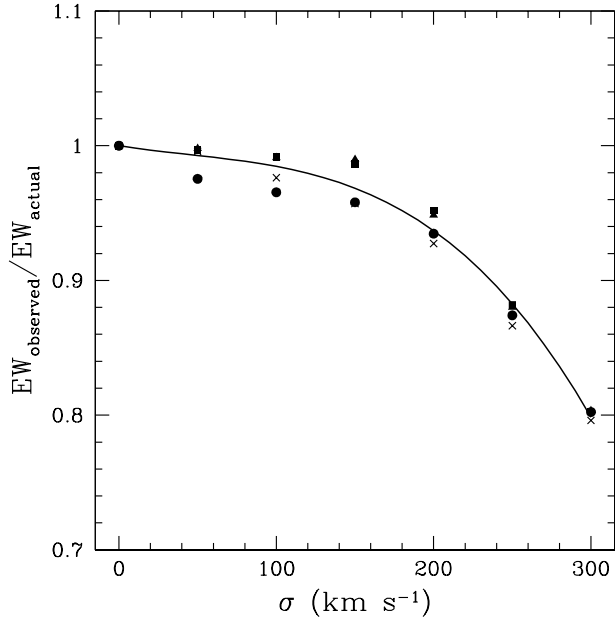


FIG. 8.— Dispersion correction to the equivalent width of the CO bandhead. The different symbols represent the change in measured equivalent width for stars with a range of equivalent widths convolved with Gaussian LOSVDs; the line is a fit to these data (described in the text) used to correct our galaxy equivalent width measurements.

### 3.3. Dust Masses

In order to ascertain the effects of dust on observed kinematics, we need to know how much dust there is in individual galaxies. In this section, we derive dust masses for our sample galaxies from IRAS flux densities according to the technique of Goudfrooij & de Jong (1995). The notation and equations below are identical to those presented in Goudfrooij & de Jong (1995). The 60 and 100  $\mu\text{m}$  flux densities are sensitive mostly to emission from cool (i.e. interstellar) dust, but are contaminated by hot (i.e. circumstellar) dust. Goudfrooij & de Jong (1995) calculated this contribution using data from Galactic Mira stars and found corrections to be

$$S(60)_{corr} = S(60) - 0.020S(12)$$

$$S(100)_{corr} = S(100) - 0.005S(12)$$

where  $S(12)$  is the 12  $\mu\text{m}$  IRAS flux density. These corrections are small for the sample galaxies.

The mass of dust  $M_d$  in a galaxy is

$$M_d = \frac{D^2 S_\nu}{\kappa_\nu B_\nu(T_d)}$$

where  $D$  is the distance to the galaxy,  $S_\nu$  is the flux density,  $B_\nu(T_d)$  is the Planck function for the dust temperature  $T_d$  at frequency  $\nu$ , and  $\kappa_\nu$  is the dust opacity

$$\kappa_\nu = \frac{4\pi a^2}{3\pi a^3 \rho_d} Q_\nu$$

where  $\rho_d$  is the specific dust grain mass density,  $a$  is the average grain radius weighted by grain volume, and  $Q_\nu$  is the grain emissivity factor. Using the grain size distribution from Mathis et al. (1977) and the values of  $Q_\nu$  from Hildebrand (1983), the dust mass in solar masses is

$$M_d = 5.1 \times 10^{-11} S_\nu D^2 \lambda^4 (\exp(1.44 \times 10^4 / \lambda T_d) - 1) M_\odot$$

where  $\lambda$  is in  $\mu\text{m}$ ,  $D$  is in Mpc, and  $S_\nu$  is in mJy.

We calculate the dust temperature as the color temperature determined from the corrected  $S(100)/S(60)$  flux ratio using the assumption of a dust grain emissivity law  $\propto \lambda^{-1}$ , typical of astronomical silicates at wavelengths  $\lambda \lesssim 200 \mu\text{m}$  (Hildebrand 1983; Rowan-Robinson 1986; Mathis & Whiffen 1989):

$$\frac{S(60)}{S(100)} = \left( \frac{\nu_{60}}{\nu_{100}} \right)^4 \frac{\exp(h\nu_{100}/kT_d) - 1}{\exp(h\nu_{60}/kT_d) - 1}$$

where  $h$  is the Planck constant,  $k$  is the Boltzmann constant, and  $\nu$  is the frequency in Hz. The temperatures calculated in this way should be regarded as estimates because a temperature distribution is surely more realistic than isothermal dust. Also, IRAS is sensitive to cool dust with  $T_d \gtrsim 25$  K, but it is predicted that much of the dust in a normal galaxy will be colder ( $\approx 10$ -20 K) and will emit more strongly at longer wavelengths. IRAS provides little information on this cold dust. Thus, the masses calculated from the IRAS color temperature are lower limits on the total dust mass in a galaxy and may be over an order of magnitude too low (Kwan & Xie 1992; Goudfrooij & de Jong 1995; Wiklind & Henkel 1995).

Table 2 lists the IRAS flux densities from Knapp et al. (1989) and the 1994 correction to those data, calculated dust temperature, and calculated dust mass for each galaxy in this sample. For galaxies which were not detected at both 60 and 100  $\mu\text{m}$ , the dust temperature is assumed to be 30 K. For galaxies that are not detected in either band, the dust mass shown is an upper limit. As expected, the calculated dust temperatures lie between 25 and 50 K, the range of IRAS's greatest sensitivity. The galaxies in this sample have a wide range of dust masses, from no detectable mass to over a million solar masses. This is, of course, a tiny fraction of the total mass of a galaxy and does not affect the potential, but may significantly affect the observed kinematics.

## 4. RESULTS AND DISCUSSION

Table 3 shows the dispersions measured from the CO bandhead and the optical dispersion measurements from the literature we use as comparisons. We are aware of the difficulties in making such comparisons; optical stellar kinematic data can vary significantly between authors, especially in the dispersion. For each galaxy, we thoroughly investigate the published kinematic data and carefully choose the measurement which is the most reliable. We make these choices based on S/N ratio, LOSVD-fitting technique, and the concordance between recent published dispersions.

The homogeneous optical sample with the most galaxies in common with this study is that of Trager et al. (1998), a large reliable study of early-type galaxies. Trager et al. (1998) has measurements for 15 of our 25 galaxies. We have worked through the analysis in the following sections using only these galaxies and their dispersions from this paper; we find no significant changes in the results reported below. Our results do not

appear to be dependent on author-to-author variations in published kinematics. The reader will notice in table 3 that we did not always choose to use the Trager et al. (1998) data when available. In some cases there are more recent measurements which appear to be better. These newer measurements are almost always consistent with Trager et al. (1998). The exception is NGC 3377. We use  $145 \pm 7 \text{ km s}^{-1}$  from Kormendy et al. (1998), while Trager et al. (1998) quotes  $126 \pm 2 \text{ km s}^{-1}$ . We believe this discrepancy is due to the high rotation of NGC 3377, which Kormendy et al. (1998) includes but Trager et al. (1998) appears not to have included.

There are three galaxies in our sample which have particularly unreliable optical measurements. These are galaxies which have especially large differences between reliable published optical dispersions, or which have only very old dispersion measurements. These galaxies are NGC 4150, NGC 5195, and NGC 6548. We repeated the analysis in the following sections without these galaxies in the sample, and again find no significant changes in our results.

For each galaxy, we choose an integrated optical dispersion measured with a similar extraction window to our measurement. However, the integrated dispersion as a function of extraction window does not vary significantly (Gebhardt et al. 2000b). Thus, any errors made due to uncertainty in the extraction window comparison will be minimal. For example, NGC 3998, which has steeply rising kinematic profiles, shows no variation in the derived velocity dispersion when we use different extraction windows. For optical dispersions without quoted uncertainties, we assume 5% of the measured value. Also, for galaxies with quoted uncertainties less than 5%, we substitute 5% of the measured value, assuming that problems with template mismatch, continuum subtraction, etc. introduce uncertainty of at least that magnitude into the optical uncertainties.

#### 4.1. Comparing IR and Optical Dispersions

Figure 9 shows the correlation between the CO dispersions and the optical dispersions. The most obvious aspect of this comparison is that most of the CO measurements are lower than the optical dispersions. The dashed line has a slope of unity, showing where the two measurements are equal, and the solid line is a fit by least squares to the data. The slope of the best fit line is  $1.189 \pm 0.084$ , which is a significant difference from unity at a  $2.25\sigma$  level. The intercept of the best fit line is  $-8.6 \pm 12.4$ , not significantly different from zero. The  $\chi^2$  of this best fit is 54.4. If we assume that there should be a correlation between the dispersions, then the 24 constraints imply that we have underestimated our uncertainties. To have a  $\chi^2$  value of 24 (matching the 24 constraints), all the errors need to be scaled up by 50%. The  $\chi^2$  of the dashed line in the plot (i.e. equality between optical and IR dispersions) is 76.2, a markedly worse fit. Increasing our uncertainties by 50% is unrealistic and the large scatter is likely real, possibly reflecting random dust distribution between galaxies.

The true ellipticals are represented in Figure 9 as open triangles while the S0s are filled circles. Our sample does not contain many true Es (because of the make-up of the SBF sample at these redshifts) so it is difficult to make definitive statements, but we examine the differences between the two populations. The true ellipticals appear to be more consistent between the infrared and optical data. The slope of the best fit line to only the ellipticals is  $0.994 \pm 0.091$ , consistent with unity, and the intercept is  $4.8 \pm 13.4$ , consistent with zero. The  $\chi^2$  of this best

fit is 1.77, which is at least consistent with the seven constraints.

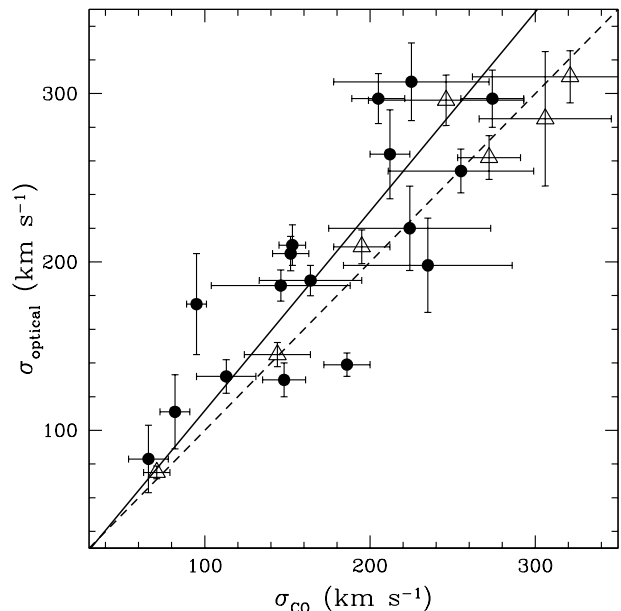


FIG. 9.— Correlation between the dispersion measured from the CO bandhead and the optical dispersion from the literature. The dashed line has a slope of unity, showing where the two measurements are equal. The solid line is the best fit to the data, as described in the text. Here and in following plots, the filled circles are S0 galaxies while the open triangles are true Es.

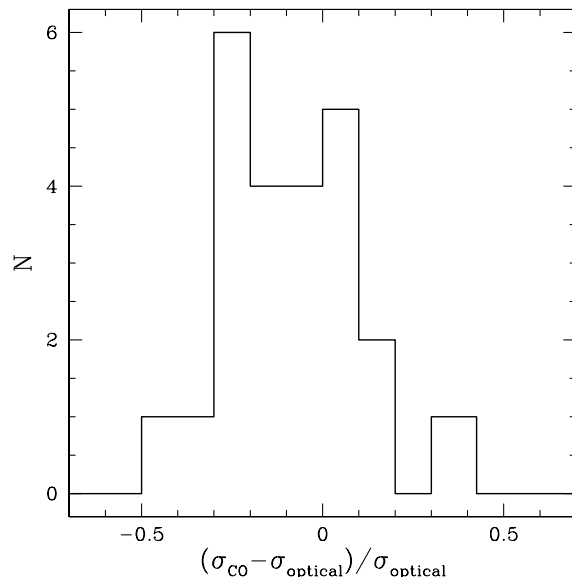


FIG. 10.— Histogram showing the number of galaxies in each bin of fractional difference between infrared and optical measurements of dispersion. The median difference is 11% smaller.

Figure 10 shows the distribution of galaxies in bins of fractional difference between the infrared and optical measurements. The dispersions measured with the CO bandhead are as much as 30% and 40% lower than their optical counterpart measurements, with the median difference being 11% lower. This is in the opposite sense to the predictions of Baes & Dejonghe (2002). Those authors's models show that dust decreases the velocity dispersion in central regions for radial and isotropic galaxies. Only for their tangential orbital structures does dust increase the central dispersion, but early-type galaxies are not usually thought to be dominated by tangential orbits. Also, the

magnitude of this effect seems to be larger than predicted by Baes & Dejonghe (2002). They predict an effect of a few percent for modest amounts of dust, and these results show an effect of up to 30% for many galaxies. Baes & Dejonghe (2002) do find an effect similar to these results (a significant decrease in the velocity dispersion) due to dust scattering, but only at several effective radii.

#### 4.2. Dust, Equivalent Widths, and Template Make-up

In Figure 11, we examine the relationship between the fractional difference between the two measurements of the dispersion and the dust mass calculated from IRAS flux densities. If it is dust which is causing the difference between the infrared and optical dispersions, then surely it is the relative amount of dust in a galaxy, not the absolute amount, which is important. To examine this, we plot the fractional difference versus the ratio of IRAS dust mass to  $B$ -band total luminosity, as quoted in RC3. This gives a rough estimate of the relative importance of dust for each galaxy. Using a  $K$ -band magnitude would be better here because dust attenuation affects the  $B$  band strongly, but some of the galaxies in our sample do not have near-IR photometric measurements in the same filter system, or even at all.

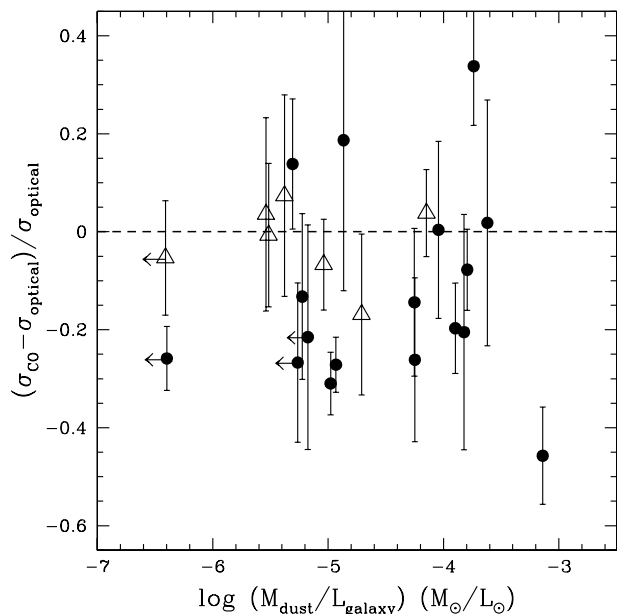


FIG. 11.— Fractional difference between infrared and optical dispersions as a function of the ratio of dust mass to  $B$ -band luminosity. The arrows indicate upper limits on the dust mass-to-light. The dashed line represents equality between the infrared and optical measurements.

We calculate the Spearman rank-order correlation coefficient ( $r_s$ ) and the probability ( $P_{r_s}$ ) to examine any statistical correlation here.  $P_{r_s} = 1$  indicates that the data are completely uncorrelated, while  $P_{r_s} = 0$  indicates complete correlation; the sign of  $r_s$  indicates correlation or anticorrelation. For the whole sample,  $P_{r_s} = 0.985$  and  $r_s = -0.0045$ ; for the sample minus the four galaxies for which the dust mass is an upper limit,  $P_{r_s} = 0.369$  and  $r_s = -0.212$ . These results imply that the dust mass-to-light ratio and the fractional difference are not likely to be correlated. There is a slight hint of an anticorrelation in the sample minus the excluded galaxies, but the evidence is not strong. The dust may be important in these differences, but there must be other effects at work besides the relative amount of dust in a galaxy. According to the models described earlier, the effect of

dust depends on the orbital structure, which could vary for the galaxies in this sample. The radial dust distribution also will change these effects and may be important in these fractional differences.

In addition, stellar population differences between the two wavelength regimes could cause such an effect. If the  $V - K$  colors of the galaxies were bluer toward their centers, the  $K$ -band light would sample less central, lower-velocity regions of the galaxy and the  $K$ -band dispersion would be lower, as found here. To test this, we are measuring  $K$ -band surface photometry of these galaxies using the recently available data of the *Two Micron All Sky Survey* (2MASS). This surface photometry has already been obtained for one galaxy in our sample, which has good agreement between its infrared and optical dispersions: M32. Peletier (1993) reports surface photometry for several optical and infrared colors and finds that M32's profile is practically flat in all colors, including the optical-infrared colors. This is consistent with negligible dust and matching optical and infrared kinematics, but does not help us understand the systematic differences between optical and infrared dispersions. Early-type galaxies are redder in their centers in optical colors, which, if also true in optical-infrared colors, would result in a change in dispersion opposite to what we find.

We can examine the relationship between equivalent width and these quantities. Table 3 shows the measured equivalent widths for the sample galaxies. In stars, the CO bandhead equivalent width increases from warmer, younger stars to cooler, older stars, with a typical early K giant having an equivalent width on the order of  $\sim 10 \text{ \AA}$  (Kleinmann & Hall 1986; Förster Schreiber 2000). Figure 12 shows the distribution of equivalent widths for this sample and how the sample properties depend on this quantity. The measured CO bandhead dispersion seems to be correlated with equivalent width, which is reasonable considering other known metallicity-dispersion relations. The probability  $P_{r_s} = 0.036$  indicates a high probability of a correlation ( $r_s = 0.438$ ). In addition, there appears to be correlation between the measured equivalent width of the galaxy and the fractional difference between the two dispersion measurements. For these quantities,  $P_{r_s} = 0.054$  and  $r_s = 0.436$ .

Also interesting is the distribution of equivalent widths of the galaxies. Almost all of the galaxies have equivalent widths over  $10 \text{ \AA}$ , to over  $20 \text{ \AA}$ . K giants have equivalent widths between  $10$  and  $15 \text{ \AA}$ , and the only stars with equivalent widths higher than about  $15 \text{ \AA}$  are M giants and K and M supergiants. The stellar population in the infrared must have a large fraction of very cool stars to match the measured equivalent widths. According to these data, the light at these wavelengths is largely dominated by M stars (probably giants). This was suggested by Rieke & Lebofsky (1979) decades ago based on near-IR photometric measurements, and provides important information about where the light is coming from at these wavelengths. By number, the effect is not as extreme. A typical M star (dwarf, giant, or supergiant) is 6 or 7 times brighter than its K star counterpart in the  $K$  band, so while finding the light dominated by M giants does imply that there is a significant population there, there is still room for other stellar types. This information must be taken into account when measuring kinematics in the near-infrared. Previous work has often used K giants for stellar templates, which easily could be the wrong choice and will effect the derived kinematics in a template-sensitive feature like the CO bandhead.

We also have information about the relative weights given to

the different template stars by the fitting program. The LOSVD fitting is free to choose from eight different template stars to achieve the best fit. The different galaxies usually use only two or three of these stars. Figure 13 shows how these weights are related to other galaxy characteristics. We quantify the make-up of the average stellar template chosen by the fitting program by the fraction of the weight given to low equivalent width (low-EW) stars. These are the template stars with an equivalent width below  $10 \text{ \AA}$ ; moderate changes in the choice of cut-off do not affect the results. The galaxies in our sample vary from giving all the weight to low-EW stars to using none of these stars. The correlation between the equivalent width of the galaxy and the weight given to templates of a certain equivalent width (upper right-hand quadrant) is expected; galaxies with high equivalent widths require templates of high equivalent width to achieve a good fit. The apparent correlation between the fractional difference between optical and IR dispersions and the fraction of low-EW templates used (upper left-hand quadrant) is just that expected from the previously mentioned correlation and the relationship between galaxy equivalent

width and dispersion differences.

Different spectral indices have been used to study the chemical history of galaxies. The  $\text{Mg}_2$  index is perhaps the most widely studied for this purpose; it is a measurement of the flux deficit in the lines compared to the neighboring continuum. Comparing this index with our infrared data may give us useful information on these aspects of galaxies. Twenty of the galaxies in our sample have  $\text{Mg}_2$  indices in the compilation of Golev & Prugniel (1998) and the updates to that compilation available on HYPERCAT (<http://www-obs.univ-lyon1.fr/hypercat/>). This catalog of published absorption-line  $\text{Mg}_2$  indices has been zero-point corrected and transformed to a homogeneous system. This facilitates comparison between different authors' measurements. We used measurements from Trager et al. (1998) when available; table 3 shows the  $\text{Mg}_2$  indices used and their sources in the literature. The actual values are taken from HYPERCAT where they have been transformed to a standard system. Figure 14 illustrates the relationships between the  $\text{Mg}_2$  index and the CO bandhead equivalent width, our velocity dispersion measurement, and the fractional differ-

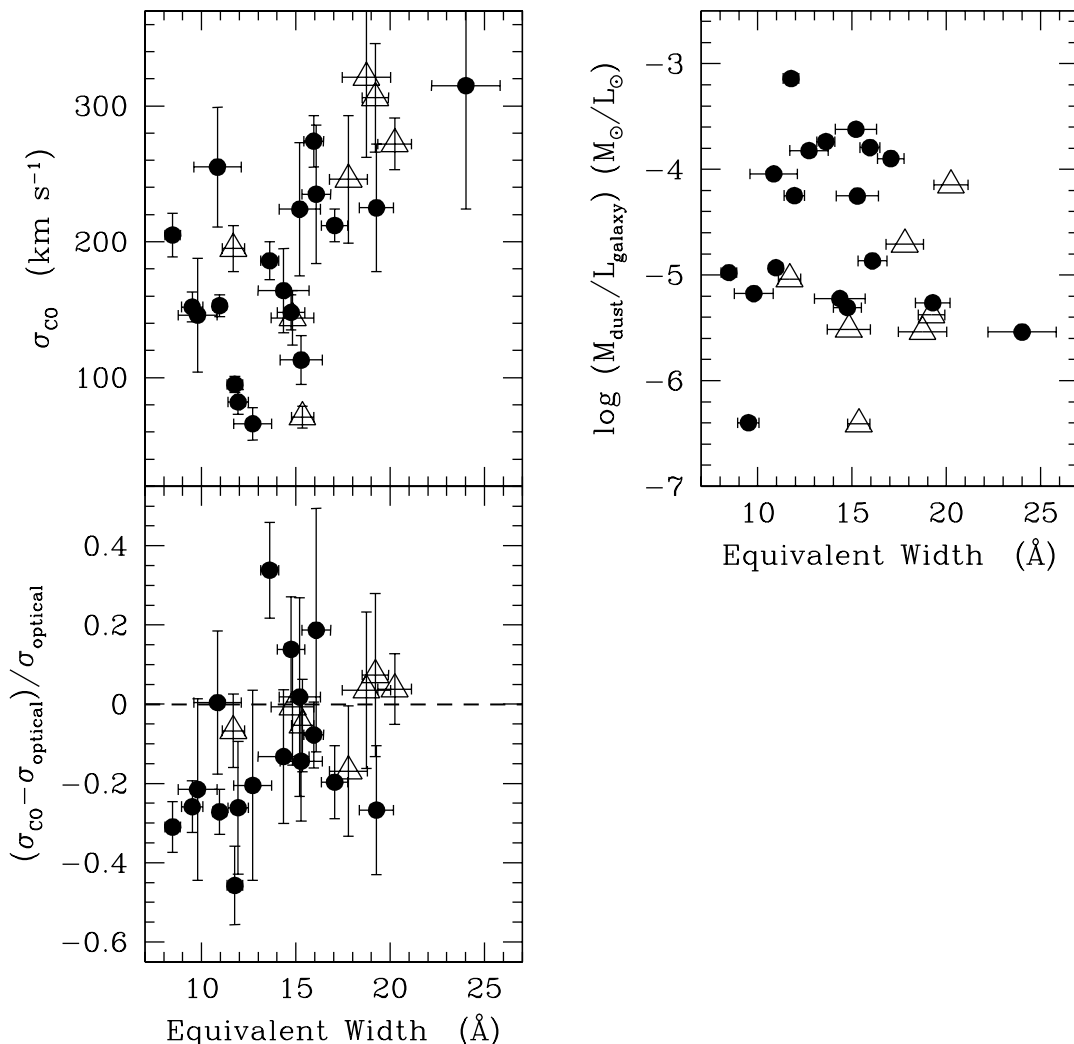


FIG. 12.— Properties of the sample galaxies as they relate to the measured CO bandhead equivalent width. Shown are the relationships between equivalent width and CO bandhead dispersion, IRAS dust mass, and fractional difference between infrared and optical dispersions.

ence between the optical and infrared dispersions. The  $Mg_2$  index appears to be tightly correlated with velocity dispersion ( $P_{r_s} = 0.105$ ,  $r_s = 0.383$ ); this is the familiar and well-studied  $Mg_2$ - $\sigma$  relation. Further investigation into the scatter, slope, etc. of this relation using infrared velocity dispersion measurements (rather than optical, as is currently done) may reveal important information about this scaling relation. The CO bandhead equivalent width is not very likely correlated with the  $Mg_2$  index ( $P_{r_s} = 0.290$ ,  $r_s = -0.249$ ). This is perhaps surprising because both the CO equivalent width and the  $Mg_2$  index appear to be significantly correlated with the velocity dispersion, which could cause them to be correlated with each other. We do not see such a relationship, which could be due to our small sample size.

#### 4.3. Messier 32

Messier 32 (NGC 221) is an important galaxy which is part of this sample. It is the compact elliptical companion of the Andromeda Galaxy here in the Local Group, and is extremely well-studied. It was not detected by IRAS and has an upper

limit on the dust mass of less than  $100 M_\odot$ . Thus, it should be an excellent candidate for calibrating this technique and exploring the case of minimal dust. It is important to keep in mind, however, that in the infrared we are looking at what may be a different stellar population with perhaps different kinematic properties. For example, if the infrared population is more centrally concentrated relative to the whole potential than the optical population, the infrared dispersion would be higher than the optical dispersion because it samples more central, higher-velocity stars.

Unfortunately, there has been some observational difficulty with this galaxy. It is at nearly zero redshift ( $cz = -145 \text{ km s}^{-1}$ ) and thus the CO bandhead falls exactly in a region of troublesome variability in atmospheric absorption. This feature was not well removed by the flattening process described above. The main reason is that NGC 221 is far brighter than any other galaxy in this sample, and thus its total integration time was less than 30 minutes. Such a short integration time made this galaxy vulnerable to problems with sky fluctuations. The other galaxies in the sample required longer exposure times which

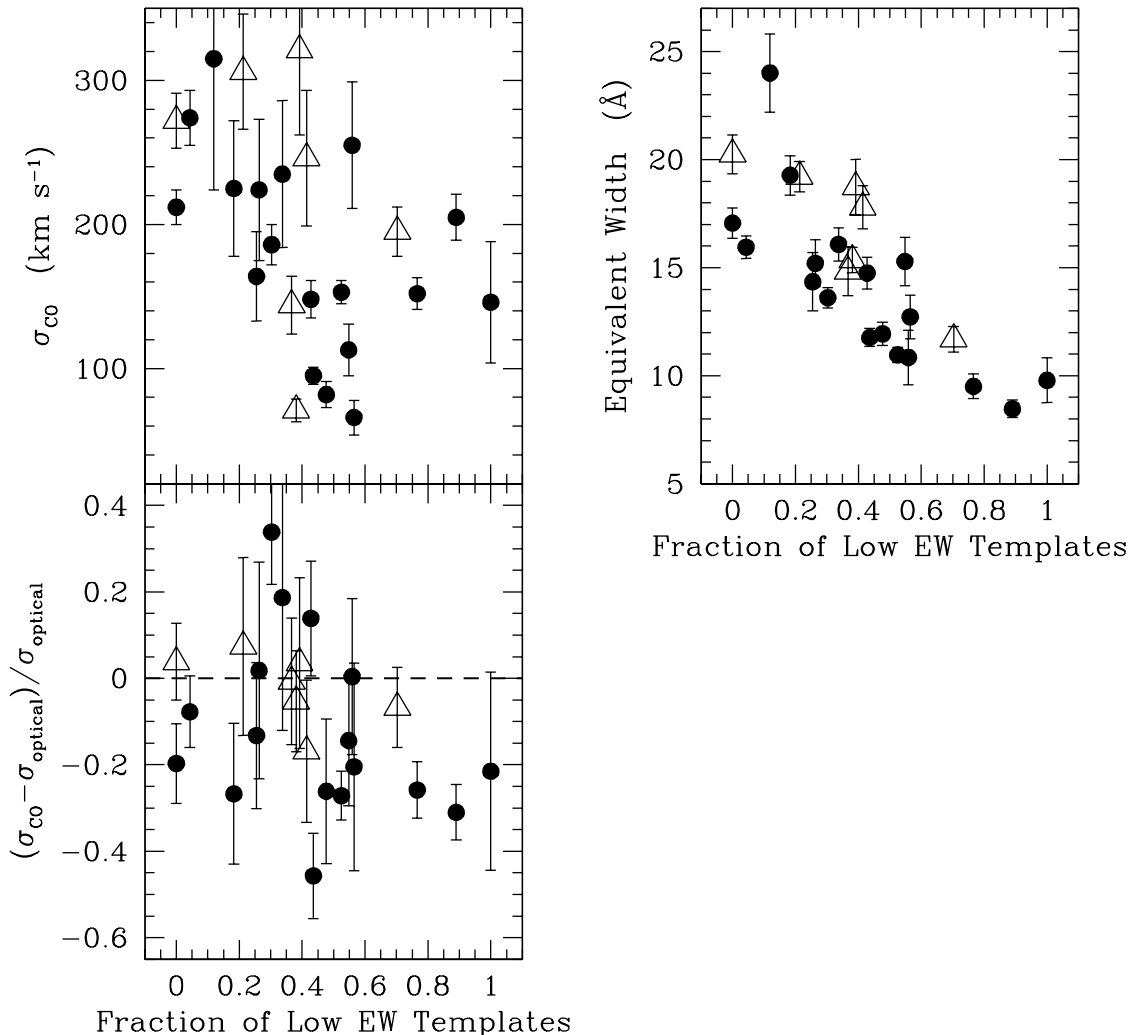


FIG. 13.— Same as Fig. 12, but for the fractional weight given to low equivalent width templates.

allowed these sky fluctuations to average out. Also, this particular atmospheric feature is not a problem for galaxies with any considerable redshift, as the feature is moved away from this region. The problem area is visible in Figure 5; it is the “bump” between 2.296 and 2.298  $\mu\text{m}$ . This region was ignored during the LOSVD fitting (a happy benefit of fitting the LOSVD directly in pixel space) and is located on the red edge (rather than the sharp blue edge which dominates the fit) but it does make it worrisome to make strong statements based on the results for this galaxy. Despite these observational difficulties, we measure a velocity dispersion of  $71 \pm 8 \text{ km s}^{-1}$ , which is very close to the value of  $75 \text{ km s}^{-1}$  from van der Marel et al. (1994). For the equivalent width of this galaxy, we choose to use the equivalent width of the fit made by the LOSVD extraction rather than of the observed spectrum, as explained in a previous section. This removes the rather large effect ( $\sim 20\%$ ) of the sky feature from the equivalent width measurement.

## 5. CONCLUSIONS

In this project, we have observed 25 nearby early-type galaxies and measured their stellar kinematics using the 2.29  $\mu\text{m}$  (2-0)  $^{12}\text{CO}$  absorption bandhead. We compare the infrared velocity dispersions of these galaxies to optical dispersions from the literature and find that the IR dispersions are generally shifted to lower values relative to the optical dispersions, between 5 and 30% for most galaxies. However, this effect is mainly driven by the S0 galaxies; pure ellipticals tend to have nearly zero offset, on average. If dust in S0 galaxies exists mainly in a disk which is cospatial with the stellar disk, optical dispersions will be biased against measuring light from this cold component and hence will come from the hot bulge component. This may explain the effect we see, since we find lower CO dispersions for lenticular galaxies, but it is currently unclear how dust is distributed in galaxies. More data is needed on the dust content and distribution of galaxies to fully understand this.

We have calculated the dust masses implied by IRAS flux densities for these galaxies and examined the relationship be-

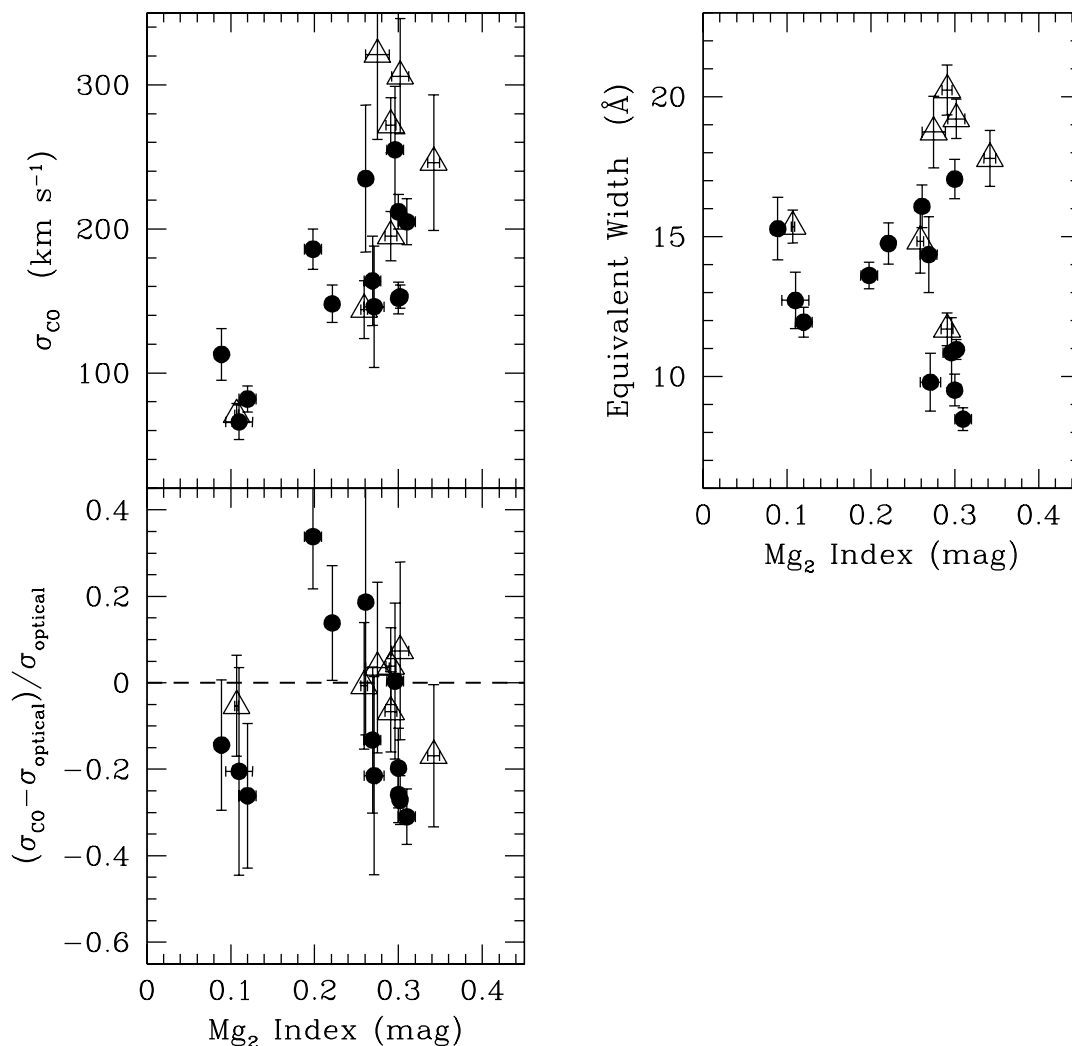


FIG. 14.— Properties of the sample galaxies as they relate to the  $\text{Mg}_2$  index (from the literature). Shown are the  $\text{Mg}_2$  index versus CO bandhead dispersion, CO bandhead equivalent width, and fractional difference between infrared and optical dispersions.

tween the differences in optical versus infrared dispersions and the amount of dust in a galaxy. We do not find a strong relationship, but dust may still be an important contributor to these differences. Both the amount and distribution of the dust can affect any differences in the mean dispersion. We have also calculated the equivalent width of this feature and compared it to other galaxy properties. The equivalent widths of the galaxies are quite high, indicating that the light is dominated by very cool (i.e. M) stars.

There are many extensions to be made from this first study. Because of the technique used to deconvolve the galaxy spectra, we are able to exploit the full LOSVDs, not just the dispersions. There is more kinematic information in the fits to these data than just the width of the LOSVD. Future work will be able to utilize the higher moments of the LOSVD to examine more detailed kinematics of sample galaxies. These higher moments are helpful to understand the orbits in galaxies. An-

other important next step in this analysis will be to combine kinematic information with infrared photometry. *2MASS* has already observed most of the galaxies in this early-type sample, as well as the late-type galaxies mentioned above, and makes these images freely available. We can use this photometry, in conjunction with optical images, to constrain infrared vs. optical stellar population differences and dust distributions. Also, we can construct an all-infrared Fundamental Plane, utilizing kinematic and photometric *K*-band data, to explore regularity in galaxy formation and evolution.

We would like to thank Dan Lester for his help and input as we have begun using CoolSpec. We gratefully acknowledge McDonald Observatory. This research project is supported by the Texas Advanced Research Program and Grant No. 003658-0243-2001.

#### REFERENCES

- Baes, M., & Dejonghe, H. 2000, *MNRAS*, 313, 153  
 Baes, M., Dejonghe, H., & De Rijcke, S. 2000, *MNRAS*, 318, 798  
 Baes, M., & Dejonghe, H. 2001, *ApJ*, 563, L19  
 Baes, M. & Dejonghe, H. 2002, *MNRAS*, 335, 441  
 Barth, A. J., Ho, L. C., & Sargent, W. L. W. 2002, *AJ*, 124, 2607  
 Beers, T. C., Flynn, K., & Gebhardt, K. 1990, *AJ*, 100, 32  
 Bower, G. A. et al. 2001, *ApJ*, 550, 75  
 Burstein, D., Bertola, F., Buson, L. M., Faber, S. M., & Lauer, T. R. 1988, *ApJ*, 328, 440  
 Burstein, D., Bender, R., Faber, S., & Nolthenius, R. 1997, *AJ*, 114, 1365  
 Davies, R. L., Burstein, D., Dressler, A., Faber, S. M., Lynden-Bell, D., Terlevich, R. J., & Wegner, G. 1987, *ApJS*, 64, 581  
 di Nella, H., Garcia, A. M., Garnier, R., & Paturel, G. 1995, *A&AS*, 113, 151  
 Doyon, R., Wells, M., Wright, G., Joseph, R., Nadeau, D., & James, P. 1994, *ApJ*, 437, L23  
 Faber, S. M., Wegner, G., Burstein, D., Davies, R. L., Dressler, A., Lynden-Bell, D., & Terlevich, R. J. 1989, *ApJS*, 69, 763  
 Fisher, D. 1997, *AJ*, 113, 950  
 Fisher, D., Franx, M., & Illingworth, G. 1996, *ApJ*, 459, 110  
 Förster Schreiber, N. M. 2000, *AJ*, 120, 2089  
 Gaffney, N., Lester, D., & Telesco, C. 1993, *ApJ*, 407, L57  
 Gaffney, N., Lester, D., & Doppmann, G. 1995, *PASP*, 107, 68  
 Gebhardt, K. et al. 2000a, *AJ*, 119, 1157  
 Gebhardt, K. et al. 2000b, *ApJ*, 539, L13  
 Gebhardt, K. et al. 2003, *ApJ*, 583, 92  
 Golev, V. & Prugniel, P. 1998, *A&AS*, 132, 255  
 Goudfrooij, P., & de Jong, T. 1995 *A&A*, 298, 784  
 Hildebrand, R. 1983 *QJRAS*, 24, 267  
 Huchra, J. P., Brodie, J. P., Caldwell, N., Christian, C., & Schommer, R. 1996, *ApJS*, 102, 29  
 Jorgensen, I., Franx, M., & Kjaergaard, P. 1995, *MNRAS*, 276, 1341  
 Kleinmann, S. G. & Hall, D. N. B. 1986, *ApJS*, 62, 501  
 Knapp, G., Guhathakurta, P., Kim, D., & Jura, M. 1989, *ApJS*, 70, 329  
 Kormendy, J. & Djorgovski, S. 1989, *ARA&A*, 27, 235  
 Kormendy, J., Bender, R., Evans, A. S., & Richstone, D. 1998, *AJ*, 115, 1823  
 Kwan, J. & Xie, S. 1992, *ApJ*, 398, 105  
 Lauer, T. R. et al. 1995, *AJ*, 110, 2622  
 Lester, D., & Gaffney, N. 1994, *ApJ*, 431, L13  
 Lester, D., Hill, G., Doppman, G. & Froning, C. 2000, *PASP*, 112, 384  
 Mathis, J., Rumpf, W., & Nordsieck, K. 1977, *ApJ*, 217, 425  
 Mathis, J., & Whiffen, G. 1989, *ApJ*, 341, 808  
 Nelson, C. H. & Whittle, M. 1995, *ApJS*, 99, 67  
 Peletier, R. F. 1993, *A&A*, 271, 51  
 Puxley, P., Doyon, R., & Ward, M. 1997, *ApJ*, 476, 120  
 Rest, A., van den Bosch, F. C., Jaffe, W., Tran, H., Tsvetanov, Z., Ford, H. C., Davies, J., & Schafer, J. 2001, *AJ*, 121, 2431  
 Rieke, G. H. & Lebofsky, M. J. 1979, *ARA&A*, 17, 477  
 Rowan-Robinson, M. 1986, *MNRAS*, 219, 737  
 Sargent, W., Schechter, P., Boksenberg, A., & Shorridge, K. 1977, *ApJ*, 212, 326  
 Shier, L., Rieke, M., & Rieke, G. 1994, *ApJ*, 433, L9  
 Shier, L., Rieke, M., & Rieke, G. 1996, *ApJ*, 470, 222  
 Tamura, M., Kleinmann, S., Scoville, N., & Joyce, R. 1991, *ApJ*, 371, 131  
 Tonry, J., & Davis, M. 1979, *AJ*, 84, 1511  
 Tonry, J. L. & Davis, M. 1981, *ApJ*, 246, 666  
 Tonry, J., Dressler, A., Blakeslee, J., Ajhar, E., Fletcher, A., Luppino, G., Metzger, M., & Moore, C. 2001, *ApJ*, 546, 681  
 Trager, S. C., Worthey, G., Faber, S. M., Burstein, D., & Gonzalez, J. J. 1998, *ApJS*, 116, 1  
 Tran, H. D., Tsvetanov, Z., Ford, H. C., Davies, J., Jaffe, W., van den Bosch, F. C., & Rest, A. 2001, *AJ*, 121, 2928  
 van der Marel, R. P., Rix, H. W., Carter, D., Franx, M., White, S. D. M., & de Zeeuw, T. 1994, *MNRAS*, 268, 521  
 van Dokkum, P. G. & Franx, M. 1995, *AJ*, 110, 2027  
 Wallace, L., & Hinkle, K. 1997, *ApJS*, 111, 445  
 White, S. D. M., Davis, M., Huchra, J., & Latham, D. 1983, *MNRAS*, 203, 701  
 Wiklund, T., & Henkel, C. 1995, *A&A*, 297, L71

TABLE 1  
BASIC PROPERTIES OF SAMPLE GALAXIES

Galaxy	Type	$v$ (km s <sup>-1</sup> )	$(m-M)$	$D$ (Mpc)	$M_B$ (mag)
NGC 0221	cE2	-145	24.55	0.813	-15.52
NGC 0315	E (LINER)	4942	–	70.600	-22.04
NGC 0821	E6	1735	31.91	24.099	-20.24
NGC 0984	S0	4352	–	62.171	-20.17
NGC 1023	S0	637	30.29	11.429	-19.94
NGC 1161	S0	1954	–	27.914	-20.18
NGC 1400	S0	558	32.11	26.424	-20.19
NGC 1407	E0	1779	32.30	28.840	-21.59
NGC 2110	S0 (Sy2)	2335	–	33.357	-18.62
NGC 2293	S0 pec	2037	31.16	17.061	-18.88
NGC 2380	S0	1782	32.05	25.704	-19.78
NGC 2681	S0/a	692	31.18	17.219	-20.09
NGC 2768	S0	1373	31.75	22.387	-20.91
NGC 2787	S0 (LINER)	696	29.37	7.482	-17.55
NGC 2974	E4	2072	31.66	21.478	-19.79
NGC 3377	E5-6	665	30.25	11.220	-19.01
NGC 3998	S0 (Sy1)	1040	30.75	14.125	-19.14
NGC 4150	S0	226	30.69	13.740	-18.25
NGC 5195	S0 pec (LINER)	465	29.42	7.656	-18.97
NGC 5866	S0 (LINER)	672	30.93	15.346	-20.19
NGC 6548	S0	2174	31.81	23.014	-19.08
NGC 6703	S0	2461	32.13	26.669	-19.81
NGC 7332	S0 pec	1172	31.81	23.014	-19.79
NGC 7619	E	3762	33.62	52.966	-21.52
NGC 7743	S0+ (Sy2)	1710	31.58	20.701	-19.20

TABLE 2  
IRAS FLUXES AND DUST CHARACTERISTICS OF SAMPLE GALAXIES

Galaxy	$S(60)$ (mJy)	$S(100)$ (mJy)	$T_d$ (K)	$\log M_d$ ( $M_\odot$ )	$\log (M_d/L_{galaxy,B})$ ( $M_\odot/L_\odot$ )
NGC 0221	<85	<1412	–	<1.99	<-6.41
NGC 0315	310	400	42.3	5.47	-5.54
NGC 0821	<41	500	–	5.25	-5.04
NGC 0984	140	140	48.0	4.72	-5.54
NGC 1023	<32	<75	–	<3.77	<-6.40
NGC 1161	1945	<9358	–	6.47	-3.79
NGC 1400	740	3280	27.2	6.37	-3.90
NGC 1407	140	480	29.2	5.45	-5.38
NGC 2110	4129	5676	41.1	6.02	-3.62
NGC 2293	380	2810	–	5.70	-4.04
NGC 2380	60	<388	–	4.88	-5.22
NGC 2681	6186	11770	35.9	5.98	-4.25
NGC 2768	390	1370	29.1	5.69	-4.87
NGC 2787	600	1180	35.5	4.28	-4.93
NGC 2974	420	1900	27.0	5.96	-4.15
NGC 3377	140	350	32.4	4.28	-5.52
NGC 3998	550	1150	34.6	4.87	-4.98
NGC 4150	1220	2670	34.1	5.24	-4.25
NGC 5195	38010	<511	–	6.64	-3.14
NGC 5866	5070	18680	28.7	6.53	-3.74
NGC 6548	<35	<119	–	<4.56	<-5.26
NGC 6703	<66	<200	–	<4.94	<-5.18
NGC 7332	210	410	35.5	4.80	-5.31
NGC 7619	<37	710	–	6.09	-4.71
NGC 7743	920	3400	28.7	6.05	-3.82

TABLE 3  
DERIVED QUANTITIES FROM OBSERVED SPECTRA AND PROPERTIES GATHERED FROM THE LITERATURE

Galaxy	Total Exposure Time (minutes)	S/N (pixel <sup>-1</sup> )	Extraction Window	Equivalent Width (Å)	$\sigma_{co}$ (km s <sup>-1</sup> )	$\sigma_{optical}$ (km s <sup>-1</sup> )	Mg <sub>2</sub> Index (mag)
NGC 0221	24	27	1.8'' × 14.0''	15.4 ± 0.59	71 ± 8	75 ± 4 <sup>a</sup>	0.107 ± 0.002 <sup>b</sup>
NGC 0315	160	13	1.8'' × 15.4''	18.7 ± 1.3	321 ± 59	310 ± 16 <sup>b</sup>	0.275 ± 0.014 <sup>b</sup>
NGC 0821	96	30	1.8'' × 11.9''	11.7 ± 0.58	195 ± 17	209 ± 10 <sup>c</sup>	0.291 ± 0.007 <sup>b</sup>
NGC 0984	168	8	1.8'' × 14.7''	24.0 ± 1.8	315 ± 91	–	–
NGC 1023	48	28	1.8'' × 17.5''	9.5 ± 0.57	152 ± 11	205 ± 10 <sup>d</sup>	0.340 ± 0.005 <sup>b</sup>
NGC 1161	72	32	1.8'' × 14.0''	15.9 ± 0.52	274 ± 19	297 ± 17 <sup>e</sup>	–
NGC 1400	40	26	1.8'' × 10.5''	17.1 ± 0.70	212 ± 12	264 ± 26 <sup>b</sup>	0.300 ± 0.007 <sup>b</sup>
NGC 1407	240	29	1.8'' × 17.5''	19.2 ± 0.70	306 ± 40	285 ± 40 <sup>b</sup>	0.302 ± 0.010 <sup>b</sup>
NGC 2110	120	12	1.8'' × 12.6''	15.2 ± 1.1	224 ± 49	220 ± 25 <sup>f</sup>	–
NGC 2293	120	14	1.8'' × 14.0''	10.8 ± 1.3	255 ± 44	254 ± 13 <sup>g</sup>	0.296 ± 0.010 <sup>m</sup>
NGC 2380	96	18	1.8'' × 10.5''	14.4 ± 1.4	164 ± 31	189 ± 9 <sup>h</sup>	0.269 ± 0.010 <sup>m</sup>
NGC 2681	120	31	1.8'' × 17.5''	11.9 ± 0.54	82 ± 9	111 ± 22 <sup>b</sup>	0.120 ± 0.010 <sup>n</sup>
NGC 2768	120	7	1.8'' × 11.2''	16.0 ± 0.77	235 ± 51	198 ± 28 <sup>b</sup>	0.261 ± 0.006 <sup>b</sup>
NGC 2787	72	48	1.8'' × 17.5''	11.0 ± 0.35	153 ± 8	210 ± 12 <sup>b</sup>	0.302 ± 0.007 <sup>b</sup>
NGC 2974	144	21	1.8'' × 14.0''	20.2 ± 0.89	272 ± 19	262 ± 13 <sup>g</sup>	0.291 ± 0.006 <sup>b</sup>
NGC 3377	166	10	1.8'' × 10.5''	14.8 ± 1.1	144 ± 20	145 ± 7 <sup>i</sup>	0.259 ± 0.004 <sup>b</sup>
NGC 3998	72	39	1.8'' × 10.5''	8.5 ± 0.41	205 ± 16	297 ± 15 <sup>j</sup>	0.310 ± 0.010 <sup>o</sup>
NGC 4150	72	8	1.8'' × 7.0''	15.3 ± 1.1	113 ± 18	132 ± 10 <sup>k</sup>	0.089 ± 0.005 <sup>b</sup>
NGC 5195	72	35	1.8'' × 7.0''	11.8 ± 0.42	95 ± 6	175 ± 30 <sup>l</sup>	–
NGC 5866	128	40	1.8'' × 14.0''	13.6 ± 0.47	186 ± 14	139 ± 7 <sup>j</sup>	0.198 ± 0.010 <sup>o</sup>
NGC 6548	296	13	1.8'' × 6.3''	19.3 ± 0.91	225 ± 47	307 ± 23 <sup>e</sup>	–
NGC 6703	208	7	1.8'' × 9.1''	9.8 ± 1.0	146 ± 42	186 ± 9 <sup>j</sup>	0.271 ± 0.012 <sup>b</sup>
NGC 7332	96	18	1.8'' × 6.3''	17.8 ± 0.73	148 ± 13	130 ± 10 <sup>b</sup>	0.221 ± 0.007 <sup>b</sup>
NGC 7619	96	12	1.8'' × 14.0''	17.8 ± 1.0	246 ± 47	296 ± 15 <sup>g</sup>	0.342 ± 0.007 <sup>b</sup>
NGC 7743	120	18	1.8'' × 4.2''	12.7 ± 1.0	66 ± 12	83 ± 20 <sup>f</sup>	0.110 ± 0.016 <sup>p</sup>

References. — (a) van der Marel et al. (1994); (b) Trager et al. (1998); (c) Gebhardt et al. (2003); (d) Bower et al. (2001); (e) Tonry & Davis (1981); (f) Nelson & Whittle (1995); (g) Jorgensen, Franx, & Kjaergaard (1995); (h) Davies et al. (1987); (i) Kormendy et al. (1998); (j) Fisher (1997); (k) di Nella et al. (1995); (l) White et al. (1983); (m) Faber et al. (1989); (n) Burstein et al. (1988); (o) Fisher, Franx, & Illingworth (1996); (p) Huchra et al. (1996);